

CrystEngComm

Accepted Manuscript



This is an *Accepted Manuscript*, which has been through the Royal Society of Chemistry peer review process and has been accepted for publication.

Accepted Manuscripts are published online shortly after acceptance, before technical editing, formatting and proof reading. Using this free service, authors can make their results available to the community, in citable form, before we publish the edited article. We will replace this *Accepted Manuscript* with the edited and formatted *Advance Article* as soon as it is available.

You can find more information about *Accepted Manuscripts* in the [Information for Authors](#).

Please note that technical editing may introduce minor changes to the text and/or graphics, which may alter content. The journal's standard [Terms & Conditions](#) and the [Ethical guidelines](#) still apply. In no event shall the Royal Society of Chemistry be held responsible for any errors or omissions in this *Accepted Manuscript* or any consequences arising from the use of any information it contains.

Cite this: DOI: 10.1039/c0xx00000x

www.rsc.org/xxxxxx

ARTICLE TYPE

Cu^{II}-PDC-bpe frameworks (PDC=2,5-pyridinedicarboxylate, bpe=1,2-di(4-pyridyl)ethylene): mapping of herringbone-type structures

Francisco Llano-Tomé,^a Begoña Bazán,^{a,b*} Miren-Karmele Urriaga,^a Gotzone Barandika,^c Luis Lezama^{b,d} and María-Isabel Arriortua^{a,b}

Received (in XXX, XXX) Xth XXXXXXXXX 20XX, Accepted Xth XXXXXXXXX 20XX

DOI: 10.1039/b000000x

Solid coordination frameworks (SCF) are crystalline materials based on connections between metal ions through organic ligands. In this sense, combination of polycarboxylate anions and dipyriddy ligands is an effective strategy to produce extended structures. In this context, this work is focused on two novel Cu^{II}-based SCFs exhibiting PDC (2,5-pyridinedicarboxylate) and bpe (1,2-di(4-pyridyl)ethylene): Cu₂[(PDC)₂(bpe)(H₂O)₂]·3H₂O·DMF (**1**), and Cu[(PDC)(bpe)_{0.5}(H₂O)]·2H₂O (**2**), where DMF is dimethylformamide. Both compounds were synthesized by slow evaporation, and their crystal structures were determined by X-ray diffraction. Further structural, thermal and magnetic characterization was carried out by means of IR, TG/DTG, DTA analysis, EPR, and measurements of the magnetic susceptibility. The crystallographic analysis revealed that compounds **1** and **2** can be described as herringbone-type layers formed by helicoidal Cu-PDC-Cu chains connected through bpe ligands. Solvent molecules are crystallized between the layers, providing the inter-layer connections through hydrogen bonds. Differences between both compounds are attributable to those solvent molecules, being indicative of the flexibility of this type of SCFs. On the other hand, due to the variety of structures found in literature that have been described as “herringbone arrays”, this work also presents a crystallochemical study based on them. The study considers stoichiometry and structural parameters leading to the identification of two types of herringbone arrays depending on the number of connections for the metal nodes (i.e. 3- and 4-connected).

Introduction

Solid coordination frameworks (SCF), also known as metal-organic frameworks (MOFs), have evolved over the last decade thanks to the variety of molecular complexes that can be formed using a broad type of organic ligands and metal ions.¹⁻⁴ Their structural features, including large cavities and high surface

areas, have opened a wide range of applications⁵ in fields like gas storage⁶⁻⁸, gas separation^{9,10}, heterogeneous catalysis¹¹⁻¹⁴, drug delivery¹⁵⁻¹⁷, chemical sensing¹⁸⁻²⁰, nonlinear optics^{21,22} and biomedical imaging.²³

One of the interesting points about these materials is the flexibility of the crystalline structures to allow the exchange of different solvents in host-guest chemistry.²⁴ The structural versatility of these molecular scaffolds is based on the large amount of available ligands to create infinite topologies, being polycarboxylate spacers some of the most used ligands. Among them, 2,5-pyridinedicarboxylate (PDC) can be mentioned as it is a non-centrosymmetric ligand, exhibiting five potential donor atoms. In fact, this ligand has been observed to produce up to twenty three coordination modes, and we first reported four of them, as a part of our research on PDC ligand.²⁵⁻²⁸ In this sense, we have been focusing our work on combinations of PDC with dipyriddy ligands. Thus, the work herein presented is devoted to the PDC-bpe combination (bpe=1,2-di(4-pyridyl)ethylene). As observed in scheme 1, where the Lewis structure for both ligands has been drawn, bpe can be found as two geometric isomers, *anti* and *gauche*, being the *anti* one the most habitual.

The PDC-bpe combination has been poorly explored in literature

^aDepartamento de Mineralogía y Petrología, Facultad de Ciencia y Tecnología, Universidad del País Vasco (UPV/EHU), Apdo 644, 48080 Bilbao, Spain.

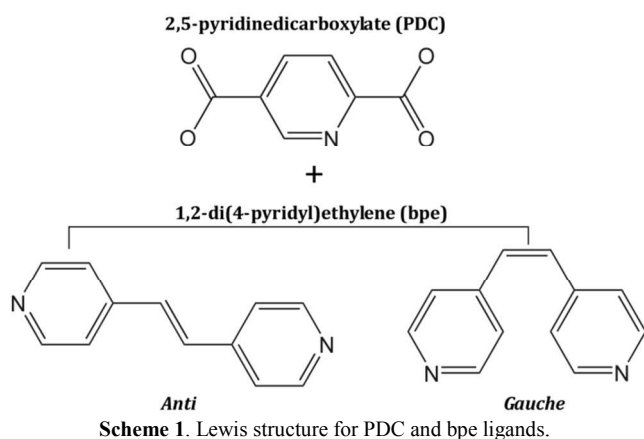
^bBCMaterials Parque Tecnológico de Zamudio, Ibaizabal Bidea, Edificio 500-Planta 1, 48160, Derio, Spain.

^cDepartamento de Química Inorgánica, Facultad de Farmacia, Universidad del País Vasco (UPV/EHU), Paseo de la Universidad, 7, 01006 Vitoria-Gasteiz, Spain.

^dDepartamento de Química Inorgánica, Facultad de Ciencia y Tecnología, Universidad del País Vasco (UPV/EHU), Apdo 644, 48080 Bilbao, Spain.

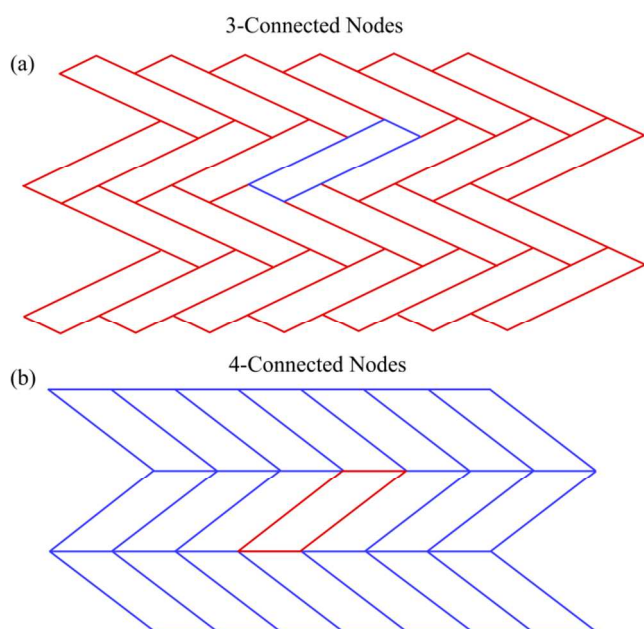
†Electronic Supplementary Information (ESI) available: Crystallographic data, IR, TGA, Distortion modes Diagram. CCDC: 997147 and 997148.

For ESI and crystallographic data in CIF or other electronic format see DOI: 10.1039/b000000x/



as concluded by the fact that just two isostructural compounds (with Co^{II} and Zn^{II}) have been reported so far exhibiting this combination.²⁹ Thus, this work reports on two novel Cu^{II} -based compounds with PDC and bpe: $\text{Cu}_2[(\text{PDC})_2(\text{bpe})(\text{H}_2\text{O})_2] \cdot 3\text{H}_2\text{O} \cdot \text{DMF}(\mathbf{1})$, and $\text{Cu}[(\text{PDC})(\text{bpe})_{0.5}(\text{H}_2\text{O})] \cdot 2\text{H}_2\text{O}(\mathbf{2})$, where DMF is dimethylformamide. Both compounds were synthesized by slow evaporation, and their crystal structures were determined by X-ray diffraction. Further structural, thermal and magnetic characterization was carried out by means of IR, TG/DTG, DTA analysis, EPR, and measurements of the magnetic susceptibility. The crystallographic analysis revealed that compounds **1** and **2** can be described as herringbone-type layers.

The term “herringbone” is being used in literature to describe a variety of 2D arrays concerning both four-connected nodes (4-c)^{30–33} and three-connected nodes (3-c).^{34–42} Scheme 2 shows that both arrays consist of the 2D packing of four-vertex polygons that exhibit nodes with three (3-c) and four connections (4-c), respectively.



Scheme 2. 2D Herringbone arrays based on four-vertex polygons. Nodes can be (a) three-connected and (b) four-connected (4-c).

Thus, as far as we are concerned, no distinction between those possibilities has been done so far when describing 2D arrays as herringbone layers. Therefore, this work also presents a crystallochemical study stating the differences.

Additionally, as compounds **1** and **2** can be described as 3-c herringbone arrays, the study has been extended to other possible 3-c planar arrays. The conclusions lead to the identification of the structural features defining the 3-c herringbone arrays. Finally, several 3-c herringbone arrays found in literature have been mapped (including compounds **1** and **2**). This mapping reveals the most favored structural features for this type of compounds.

Experimental section

General

All solvents and chemicals were used as received from reliable commercial sources. The reactants 2,5-pyridinedicarboxylic acid (H_2PDC), 1,2-di(4-pyridyl)ethene (bpe), copper(II) nitrate hexahydrate 99%, triethylamine (Et_3N), and the solvent N,N -dimethylformamide (DMF) 99.8% were purchased from Sigma-Aldrich Co. The nitric acid 65% (HNO_3) was purchased from Panreac.

Synthesis of compound **1**

H_2PDC (40.4 mg, 0.25 mmol), bpe (46.3 mg, 0.25 mmol) and $\text{Cu}(\text{NO}_3)_2 \cdot 6\text{H}_2\text{O}$ (93.3 mg, 0.5 mmol) were dissolved in a solvent mixture of DMF/ H_2O (10/10 mL) after stirring for 1h at RT. The pH value was adjusted to 4.5 using Et_3N and HNO_3 (0.5 M). The resulting solution was sealed in a teflon-lined autoclave for microwaves (XP1500), heating at 140°C during 45 min in order to improve the solubility of the reagents. Then, the solution was filtered and dropped in a glass crystallizing dish. After twelve hours, blue prismatic crystals were obtained. The sample was washed and dried with ethanol, collecting a crystal for X-ray diffraction experiment. The density was measured by the flotation method in a mixture of bromoform/chloroform being $1.68(5) \text{ g} \cdot \text{cm}^{-3}$ (Found: C, 42.5(2); H, 3.59(2); N, 8.64(3). Calc. for $\text{C}_{29}\text{H}_{33}\text{Cu}_2\text{N}_5\text{O}_{14}$: C, 43.57; H, 3.75; N, 8.75. IR: $\nu_{\text{max}}/\text{cm}^{-1}$ 3415 (OH), 1656 and 1608 (aroC-C), 1286 (C-N), 1561 (asCOO), 1428, 1387 and 1352 (sCOO), 833, 770 and 692 (C-H) and 550–534 (Cu-N) (Fig.S1, ESI†).

Synthesis of compound **2**

H_2PDC (122.1 mg, 0.75 mmol), bpe (176.4 mg, 1 mmol) and $\text{Cu}(\text{NO}_3)_2 \cdot 6\text{H}_2\text{O}$ (187 mg, 1 mmol) were dissolved in a solvent mixture of $\text{H}_2\text{O}/\text{MeOH}$ (20/10 mL) after stirring for 30 min at RT. The pH value was adjusted to 4.5 using HNO_3 (0.5 M). The resulting solution was sealed in a teflon-lined autoclave and heated at 120°C for 72 h. The solution was slowly cooled at RT and filtered, pouring into a glass crystallized dish. After one day, light-green prismatic crystals were obtained. The sample was washed and dried with ethanol allowing the collection of one single-crystal for X-ray diffraction experiment. The density was measured by the flotation method in a mixture of bromoform/chloroform being $1.61(5) \text{ g} \cdot \text{cm}^{-3}$ (Found: C, 41.87(2); H, 3.65(2); N, 7.50(3). Calc. for $\text{C}_{13}\text{H}_{10}\text{CuN}_2\text{O}_7$: C, 42.57; H, 3.54; N, 7.63. IR: $\nu_{\text{max}}/\text{cm}^{-1}$ 3410 (OH), 1656 and 1617 (aroC-C), 1281 (C-N), 1569–1560 (asCOO), 1428, 1390 and 1348 (sCOO), 834, 765 and 687 (C-H) and 551–534 (Cu-N) (Fig.S2, ESI†).

Single-crystal X-ray diffraction

Prismatic single-crystals of compounds **1** and **2** with dimensions given in Table 1 were selected under polarizing microscope and mounted on MicroMounts. Single-crystal data were collected at 100 K on an Agilent Technologies Supernova single source diffractometer with Cu-K α radiation (1.54184 Å) for compounds **1** and **2**. Details of crystal data and some features of the structures refinements are reported in Table 1, and selected bond length and angles are listed in Table S1 and S2 (ESI \dagger).

Table 1. Details of the crystal data, structural resolution and refinement procedure for **1** and **2**.

Compounds	1	2
Formula	C ₂₉ H ₃₃ N ₅ O ₁₄ Cu ₂	C ₁₃ H ₁₀ N ₂ O ₇ Cu
FW, g·mol ⁻¹	802.68	369.77
Crystal system	Monoclinic	Monoclinic
S.G., (n ^o)	<i>Pn</i> , (7)	<i>P2₁/n</i> , (15)
<i>a</i> , Å	11.4682(2)	11.3256(3)
<i>b</i> , Å	8.8977(1)	8.9352(2)
<i>c</i> , Å	15.6872(2)	15.1672(4)
β , °	94.074(1)	93.037(3)
<i>V</i> , Å ³	1596.69(1)	1532.71(3)
<i>Z</i> , <i>F</i> (000)	2, 824	4, 748
ρ_{obs} , ρ_{cal} , g·cm ⁻³	1.68(5), 1.67	1.61(5), 1.60
μ , mm ⁻¹	2.341	2.380
Crystal size, mm	0.096 x 0.064 x 0.035	0.108 x 0.072 x 0.03
Radiation, λ , Å	1.54184	1.54184
Temperature, K	100(10)	100(10)
Reflections collected, unique	11540, 4648	11849, 3051
Limiting indices	(<i>R_{int}</i> = 0.027) -14 <= <i>h</i> <= 12 -10 <= <i>k</i> <= 11 -17 <= <i>l</i> <= 19	(<i>R_{int}</i> = 0.029) -14 <= <i>h</i> <= 14 -6 <= <i>k</i> <= 10 -18 <= <i>l</i> <= 18
Final <i>R</i> indices	<i>R</i> ₁ = 0.029, w <i>R</i> ₂ = 0.076	<i>R</i> ₁ = 0.048, w <i>R</i> ₂ = 0.137
<i>R</i> indices (all data) ^a	<i>R</i> ₁ = 0.031, w <i>R</i> ₂ = 0.078	<i>R</i> ₁ = 0.054, w <i>R</i> ₂ = 0.144
Goodness of fit on <i>F</i> ²	1.041	1.014
Parameters /restraints	519 /14	232/3
L. Diff. peak and hole (e Å ⁻³)	0.776, -0.355	0.911, -0.534

Lattice constants were obtained by using a standard program belonging to the diffractometer software, confirming at the same time the good quality of the single-crystals. The Lorentz polarization and absorption corrections were made with the diffractometer software, taking into account the size and shape of the crystals.⁴³ The structures were solved by direct methods with the SIR92⁴⁴ program, in the monoclinic *Pn* space group for compound **1**, and with the *P2₁/n* space group for compound **2**, which allowed us to obtain the position of the copper atoms, as well as oxygen and nitrogen atoms and some of the carbon atoms of both ligands of PDC and bpe of compounds **1** and **2**. The refinement of the crystal structures was performed by full matrix least-squares based on *F*², using the SHELXL-97⁴⁵ program, obtaining the remaining carbon atoms and allowing the allocation of the hydrogen atoms. Anisotropic thermal parameters were used for all non-hydrogen atoms (Fig. S3 and Fig. S4, ESI \dagger). The

hydrogen atoms belonging to the organic molecules were fixed geometrically and allowed to ride on their parent carbon atoms (C-H 0.93 Å) and refined with common isotropic displacements. The position of the hydrogen atoms bonded to the coordination water molecules of compound **1** and **2**, as well as the hydrogen atoms bonded to the crystallization water molecules of compound **1** were fixed using DFIX and DANG instructions in the refinement to adjust the O-H distance to 0.82 Å and the H-O-H angle to 112°, respectively. All the crystallization water molecules for compound **2** were disordered in two groups. The hydrogen atoms of these water molecules were not considered due to the lack of density in the residual density map. One important point is that the DMF molecules break the *P2₁/n* symmetry for compound **1**, resulting in the impossibility of locating the molecules of water and DMF in the cavities during refinement. Table S3 shows the crystallographic data corresponding to this structural resolution. This resolution permits the localization of the atoms corresponding to the layers. However, crystallization molecules of DMF and water cannot be localized. Therefore, the structure was solved in *Pn* space group.

Physicochemical characterization techniques

The thermogravimetric analysis (TGA) was performed under air atmosphere on a SDT 2960 Simultaneous DSC-TGA TA Instrument. The IR spectra were obtained with a Jasco FT/IR-6100 spectrophotometer in the 400–4000 cm⁻¹ range with pressed KBr pellets. C, H and N elemental analyses were measured using a Euro EA 3000 Elemental analyzer.

Variable temperature (5–300 K) magnetic susceptibility measurements on polycrystalline samples were carried out with a Quantum Design MPMS-7 SQUID magnetometer under a magnetic field of 0.1 T. The experimental susceptibilities were corrected for the diamagnetism of the constituent atoms by using Pascal's tables. X-band EPR measurements were carried out on a Bruker ELEXSYS 500 spectrometer with a maximum available microwave power of 200 mW and equipped with a super-high-Q resonator ER-4123-SHQ and standard Oxford low temperature devices. For Q-band studies, EPR spectra were recorded on a Bruker EMX system equipped with an ER-510-QT. The magnetic field was calibrated by a NMR probe and the frequency inside the cavity was determined with a Hewlett-Packard 5352B microwave frequency counter. Computer simulation: WINEPR-Simfonia, version 1.5, Bruker Analytische Messtechnik GmbH.

Results and discussion

Crystal structures

Crystal structures for compounds Cu₂[(PDC)₂(bpe)(H₂O)₂]·3H₂O·DMF(**1**), and Cu[(PDC)(bpe)_{0.5}(H₂O)]·2H₂O(**2**) are quite similar, so they will be described together. In fact, both compounds consist of 2D arrays of the as-called herringbone-type. These layers are interconnected via hydrogen bonds through the crystallization molecules (1 DMF and 3 water molecules per 2 Cu^{II} ions in compound **1**, and 4 water molecules per 2 Cu^{II} ions in compound **2**, giving rise to a 3D supramolecular framework (Fig. 1), with channels along the [010] direction (Table S4 and Table S5, ESI \dagger). The 2D arrays are formed by zig-zag chains of Cu-PDC-Cu.

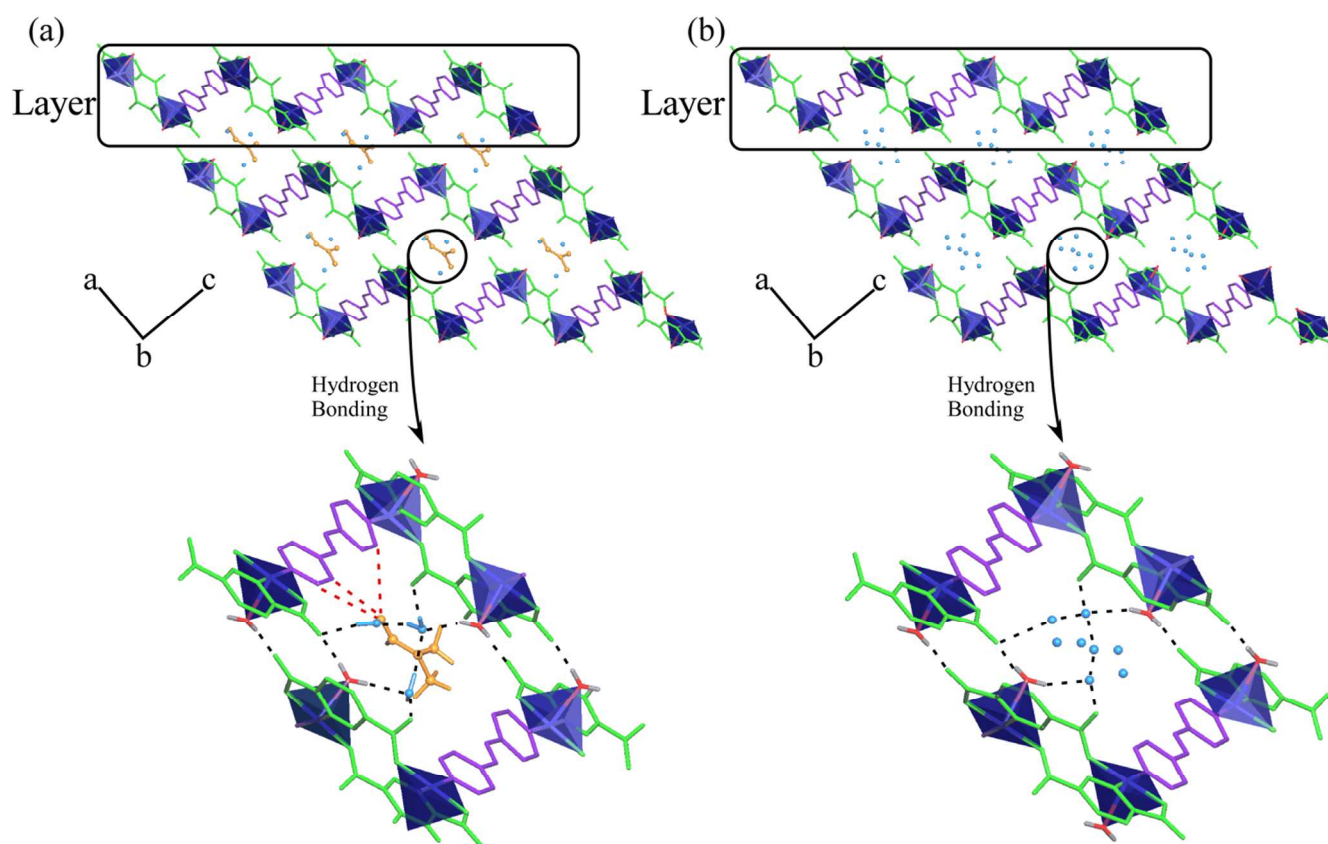


Fig. 1 3D supramolecular frameworks for compounds **1** (a) and **2** (b). The PDC and bpe ligands are colored in green and purple, respectively. (bottom left) Zoom of the crystallization molecules of DMF (orange) and water (blue) for compound **1** connected to the layers through hydrogen bonds (red and black), and water (blue) for compound **2**, and (bottom right) zoom of the disordered crystallization molecules of water (blue) for compound **2** (all hydrogen atoms are omitted for clarity).

This is reflected in the helical axis for compound **2** (space group $P2_1/n$) but, as explained above, the presence of DMF in compound **1** leads to a lower symmetry of the framework (space group Pn). These chains are interconnected through the bpe ligand producing the herringbone pattern (Fig. 2).

The torsion angles of the bpe ligand for compounds **1** and **2** are 7.15° and 1.47° , respectively. Therefore, bpe appears as the *anti* geometric isomer.

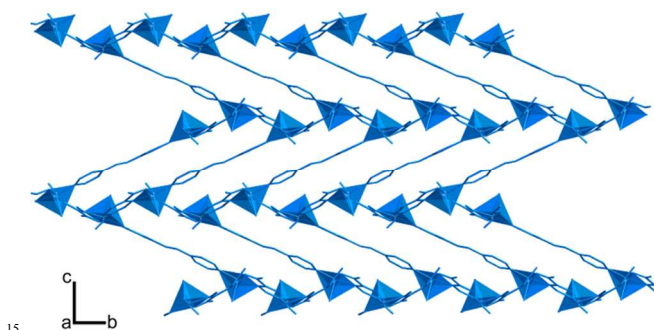


Fig. 2 2D herringbone layer observed for compound **1**.

The asymmetric unit for compound **1** is formed by two crystallographically independent Cu atoms (Cu1 and Cu2). This way, $\text{Cu1}\cdots\text{Cu2}$ and $\text{Cu2}\cdots\text{Cu1}^i$ ($i = x, -1+y, z$) distances in the chain for compound **1** are $7.271(2)$ Å and $7.235(2)$ Å,

respectively. The Cu1-Cu2-Cu1^i and $\text{Cu2}^{ii}\text{-Cu1-Cu2}$ ($ii = x, 1+y, z$) angles are the same, being $75.67^\circ(1)$ for both cases. In the case of compound **2**, the $\text{Cu1}\cdots\text{Cu1}^i$ ($i = 1/2-x, -1/2+y, 3/2-z$) distance is $7.210(5)$ Å, and the $\text{Cu1}^{ii}\text{-Cu1-Cu1}^i$ ($ii = 1/2-x, 1/2+y, 3/2-z$) angle is $76.58^\circ(5)$.

For compound **1**, as well as for compound **2**, Cu atoms have square pyramidal coordination environment, being coordinated to two oxygen atoms and a nitrogen atom (from two different PDC ligands) and to a nitrogen atom belonging to a bpe ligand in the equatorial plane and to water molecule in the apical position.

In both cases, Cu-O distances lie within the range $1.934(2)$ - $2.220(1)$ Å, and Cu-N distances exhibit values between $2.010(3)$ - $2.033(1)$ Å as reported for other complexes containing Cu^{II} (Table S1 and S2, ESI[†]). Most significant bond distances and angles are reported in Table S6 and Table S7 (ESI[†]), respectively. In summary, the difference between both compounds lies on the molecules of solvent connecting the layers being indicative of the flexibility of this type of compounds.

As previously said, there are channels along the [010] direction, and their diameter has been evaluated by means of the Voronoi-Dirichlet polyhedra, which were constructed through the Dirichlet program included in TOPOS⁴⁶ (Fig. S5, ESI[†]). As observed, both compounds show a straight channel path. The diameters (D) are quite similar: $D_{\text{max}} = 2.888$ Å (for **1**) and 2.818 Å (for **2**), and $D_{\text{min}} = 2.588$ Å (for **1**) and 2.512 Å (for **2**). In fact, compound **1** exhibits the largest cavities as corresponds to the

fact that DMF molecules are larger. As observed, the interlayer distance is consistent with the latter (Fig. S6, ESI†).

Topological features for compounds **1** and **2** were analyzed by means of the TOPOS⁴⁶ software, revealing a hcb Shubnikov hexagonal plane net (Point symbol = 6^3 and vertex symbol = [6.6.6]), corresponding to the topology shown in scheme 2a. Further discussion on topology will be done in the section devoted to the mapping of 3-c herringbone-arrays.

Distortion of coordination spheres for metal centres

Distortion of coordination polyhedra was evaluated according to Avnir^{47,48} method, based on the continuous symmetry measures (CSM), by means of SHAPE⁴⁹ program, and the results can be seen on Table 2. The projection of the as-calculated values on the distortion diagram can be seen in Fig. S7 (ESI†). As observed for the three analyzed Cu^{II} ions, distortion is on a non-Berry pathway that converts the trigonal bipyramid into a square pyramid (SPY) with a soft contribution of a vacant octahedron (VOC) distortion. In fact, for Cu1 and Cu2 in compound **1**, the axial distances (Cu1-O5=2.259(3) Å and Cu2-O6=2.216(3) Å) are longer than the equatorial ones (going from 1.947(3) Å to 2.030(3) Å). Similarly, for compound **2**, the axial distance Cu1-O1W is 2.245(3) Å and the equatorial ones go from 1.943(2) Å to 2.027(3) Å.

Table 2. Geometrical distortions of the trigonal bipyramid (TBPY) and bery square pyramid (SPY) calculated by means of Shape software.

Compounds	Pentacoordinate	S(TBPY)	S(SPY)
Compound 1	Cu(1)	5.49	1.19
	Cu(2)	5.37	1.13
Compound 2	Cu(1)	5.70	1.13

Thermogravimetry

In order to study the thermal stability of compounds **1** and **2**, thermogravimetric (TG) analysis was performed.

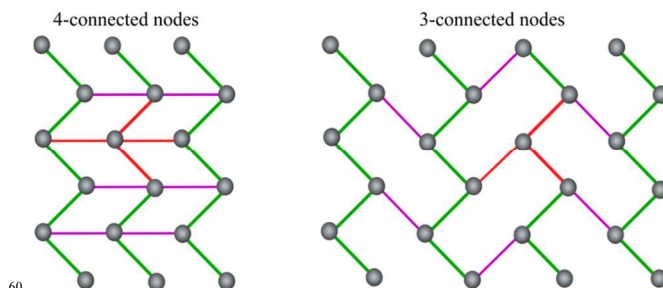
Compound **1** shows two-stages of mass loss (Fig. S8, ESI†). The first of them, starting at RT and finishing at about 165 °C, has been assigned to the removal of the crystallization and coordination molecules of water and DMF (20.3% calc. and 22.2% exp.). The second one (63.83% calc. and 62.74% exp.) is an abrupt mass loss, and corresponds to the removal of both organic ligands occurring between 255 °C and 345°C. The residue has been identified by X-ray powder diffraction as CuO.⁵¹

The TG analysis of compound **2** shows a weight loss of 15.4% from RT to 86°C (Fig. S9, ESI†), attributed to the crystallization and coordination molecules of water (14.44% calc.). The curve shows a plateau up to 280°C, when the calcination of the organic molecules takes place with a weight loss of 64.24% (68.54% calc.). The calcination product was also CuO.⁵¹

Mapping of 3-c herringbone-arrays

As said before (Scheme 2), herringbone arrays are produced by the 2D packing of four-vertex polygons that can be three- (3-c) and four-connected (4-c). If translating those topologies to an ideal array consisting of metal nodes and two organic ligands (A and B), the result is that four-vertex polygons are produced by four-metal nodes in a 4-c herringbone but by six-metal nodes for a 3-c array (Scheme 3). Both types of layers differ in

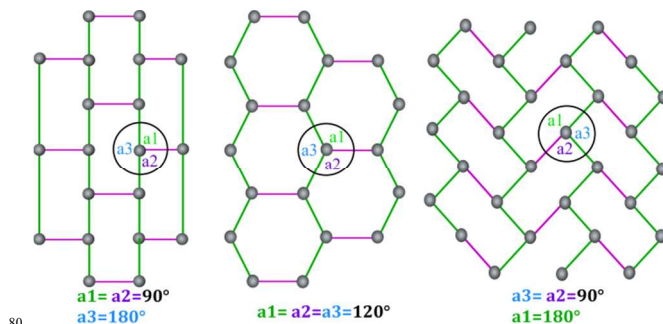
stoichiometry, being $M_1A_1B_1$ for 4-c planes, and M_2A_2B for 3-c ones. As observed in scheme 3, both types of arrays have in common the zig-zag chain (green) extending by metal nodes sharing A ligands. The connection between these chains through B ligands (purple) is the distinguishing factor between both arrays. In summary, $M_1A_1B_1$ stoichiometry in 4-c planes produces four-vertex/four-node polygons, while M_2A_2B for 3-c ones produces four-vertex/six-node polygons.



Scheme 3. (left) 4-c and (right) 3-c herringbone 2D arrays. Green and purple lines represent A and B ligands, respectively. Lines in red mark the 4-c and 3-c nodes.

Since compounds **1** and **2** exhibit 3-c herringbone planes, next discussion will be referred to 2D arrays based on 3-c nodes.

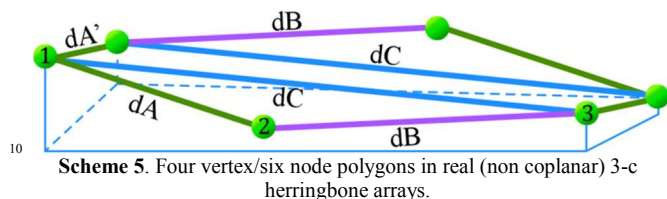
It is worth noticing that in the ideal array shown in scheme 3, all the nodes are coplanar. Additionally, distances between metal nodes through A (d_A , green) and B (d_B , purple) ligands are identical ($d_A=d_B$), producing a high-symmetry plane. If considering that an ideal geometry is highly symmetrical, the 3-c herringbone shown in scheme 3 is just one of the ideal possibilities for 3-c nodes to extend in planes and producing six-node polygons. In fact, as shown in scheme 4, there are other two ideal geometries for $d_A/d_B=1$. This way, possibility 1 is based on brick-wall sheet; possibility 2 consists of regular hexagons; and possibility 3 is a 3-c herringbone array. The “a1”, “a2” and “a3” angles defined in scheme 4 for the nodes mark the differences among these three possibilities.



Scheme 4. Possibilities for high-symmetry planes based on 3-c nodes according to angles “a1”, “a2”, and “a3”. (left) brick-wall sheet, (center) regular hexagons, and (right) herringbone array.

As observed in scheme 4, transition from hexagon-based plane to brick-wall sheet and 3-c herringbone array implies that a_2 angle goes from 120° to 90° for both cases. Therefore, a_1 - a_3 parameter becomes -90° for brick-wall sheet and +90° for 3-c herringbone array. It is also worth noticing that the hexagonal array does not admit d_A and d_B to be different. However, brick-wall sheet and 3-c herringbone array can be produced for the cases when both distances are not equal ($d_A \neq d_B$).

As mentioned before, compounds **1** and **2** exhibit 3-c herringbone planes, but their “a2”, “a1-a3” and “dA/dB” parameters are far from those corresponding to high symmetry. In fact, scheme 5 represents the real situation for both compounds where the non-coplanarity of the six nodes is observed. Thus, if we take three consecutive nodes (1, 2 and 3), dC parameter (blue line) can be defined as the distance between nodes 1 and 3 (nodes 1 and 2 being linked through A ligand, and nodes 2 and 3 being linked through B ligand).



It is also worth noticing that in real structures, two distances through the A ligand can be defined: dA and dA'. In most of the cases, both of them are quite similar. Thus, the four-vertex polygons are formed by dA'-dC-dA'-dC sides while the six-node ones are formed by dA-dB-dA'-dA-dB-dA' sides. The situation is similar for other compounds found in literature.³⁴⁻⁴² Finally, while in an ideal 3-c herringbone array the sum of dA and dB distances is dC due to coplanarity of the six nodes (dA+dB=dC), in real compounds the sum of dA and dB distances is different to dC (dA+dB≠dC). Therefore, dB* distance has also been defined (dB*=dC-dA).

Table 3 collects these angles and distances for several compounds found in literature and described as herringbone arrays.³⁴⁻⁴² The selection in Table 3 does not intend to be exhaustive since more than 2300 compounds have been found in the TOPOS⁴⁶ data base exhibiting the 3-c topology shown in scheme 1.

However, many of these topologies are referred to connections between M-A-M zig-zag chains through hydrogen bonds, and this is not the case under study in this work. On the other hand, there are singular characteristics in many of the self-named herringbone-arrays that do not fit with the description herein made such as the coordination number of the metal centers (4-c), angles M-A-M that do not lie within these herringbone arrays and the dimensionality of the frameworks.

Table 3. Structural parameters for the selected “herringbone” arrays.

Compounds	dA(Å)	dA'(Å)	dB(Å)	dC(Å)	dB*(Å)	a1(°)	a2(°)	a3(°)	a1+a2+a3
[Cu(PDC)(bpe) _{0.5} (H ₂ O)]·2H ₂ O	7.21	7.21	13.43	19.32	12.11	136.77	66.34	76.58	279.69
[Cu ₂ (PDC) ₂ (bpe)(H ₂ O) ₂]·3H ₂ O·DMF	7.27	7.23	13.44	19.42	12.15	137.19	68.07	75.67	280.93
[Zn(4,4bipyridine)(Hptc)·H ₂ O] ³⁴	5.34	5.34	11.06	15.67	10.33	143.20	76.98	84.03	304.21
[Cd(hmph)(dpa)]·H ₂ O ^{35,36}	5.62	12.06	11.88	12.58	6.97	148.27	79.77	82.07	310.11
[Zn(H ₂ MBP)(Br-IPA)] _n ·CH ₃ OH ³⁷	8.97	8.97	7.72	15.80	6.83	142.41	71.67	119.17	333.25
[Zn(H ₂ MBP)(CH ₃ -IPA)] _n ·CH ₃ OH ³⁷	9.02	9.02	7.76	15.74	6.71	139.10	74.97	121.01	335.08
[Cu ₂ (3,5-(NO ₂) ₂ sal) ₂ (4'4bipy)(H ₂ O)] _n ^{38,39}	5.02	5.02	11.11	16.00	10.98	164.09	67.02	106.78	337.89
[Pr(bib) ₂ (NO ₃) ₃] ⁴⁰	14.73	14.73	15.27	29.84	15.11	168.26	70.84	102.90	342.00
[Cd ₂ (azpy) ₃ (NO ₃) ₄]·2Me ₂ CO ⁴¹	13.44	13.44	13.66	26.67	13.23	159.52	81.38	102.68	343.58
[Cd ₂ (NO ₃) ₄ (4,4'-azpy) ₃]·CH ₂ Cl ₂ ·xH ₂ O ^{39,42}	13.15	13.15	13.31	26.00	12.85	158.62	82.54	102.90	344.06
[Co ₂ (NO ₃) ₄ (4,4'-azpy) ₃]·CH ₂ Cl ₂ ·xH ₂ O ⁴²	13.30	13.30	13.36	26.25	12.94	159.78	81.06	104.46	345.30
Zn[(H ₂ MBP)(OME-IPA)] _n (H ₂ O) ³⁷	8.57	8.57	8.12	14.88	6.30	163.35	75.88	120.39	359.62

In fact, the purpose of our selection is to be representative of similar arrays to the one found for compounds **1** and **2**. For example, one of the discarded compounds is Zn(H₂MBP)(IPA)·H₂O, described by S. Sengupta *et al.*³⁷ as herringbone together with other Zn-H₂MBP compounds. The reason for the discarding in this study is that its parameters indicate that the 3-c array is close to ideal hexagonal but tending to brick-wall sheet and not to a 3-c herringbone array (a1-a3 = -3.24°, dA/dB = 1.16, and dA/dB* = 1.17).

As previously said, the 3-c herringbone array is consistent with the M₂A₂B stoichiometry. Therefore, some explanations are required for compounds in Table 3, in order to avoid confusion.

Firstly, in compound [Zn(4,4-bipyridine)(Hptc)H₂O]_n³⁴ half of the Hptc ligands do not perform as connectors; so, the stoichiometry for the bridging ligands is in fact Zn(4,4-bipyridine)(Hptc)_{0.5}, as expected. Secondly, in compounds with Zn and H₂MBP³⁷, there are double bridges through Br-IPA, CH₃-IPA and OME-IPA ligands, so two ligands account for a single A unit.

Additionally, in compounds [M₂(NO₃)₄(4,4'-azpy)₃]·CH₂Cl₂·X(H₂O)^{39,42} (M=Cd, Co), the ligand 4,4'-azpy plays both roles (as A and B ligands); so there are three ligands per two metal ions. Thirdly, in compound [Pr(bib)₂(NO₃)₃]⁴⁰, the nitrate oxoanions do not perform as connectors, and the bib ligand acts as A and B, but establishing double bridges when performing as B.

Finally and similarly, in compound [Cd₂(azpy)₃(NO₃)₄]·2Me₂CO⁴¹, the nitrate groups are terminal ligands, and the azpy connector plays both roles as A and B ligands (with single bridges for both of them).

As observed, all the compounds in Table 3 exhibit a1+a2+a3 values distinct from the ideal value of 360°, in consistence with the lack of coplanarity. Taking into account the relationship for a1, a2 and a3 angles (Scheme 4), a2 parameter has been represented vs a1-a3 angle (Fig. 3).

As observed, most of the compounds are located on the same zone of the graph. It is also worth noticing that dispersion for a2 values (this is, the zig-zag angle for M-A-M chain) is very low (average a2 value is 74(5)°, while values of a1-a3 go from 18.09° to 61.52°, and the majority of them are located around a1-a3=60°).

Cite this: DOI: 10.1039/c0xx00000x

www.rsc.org/xxxxxx

ARTICLE TYPE

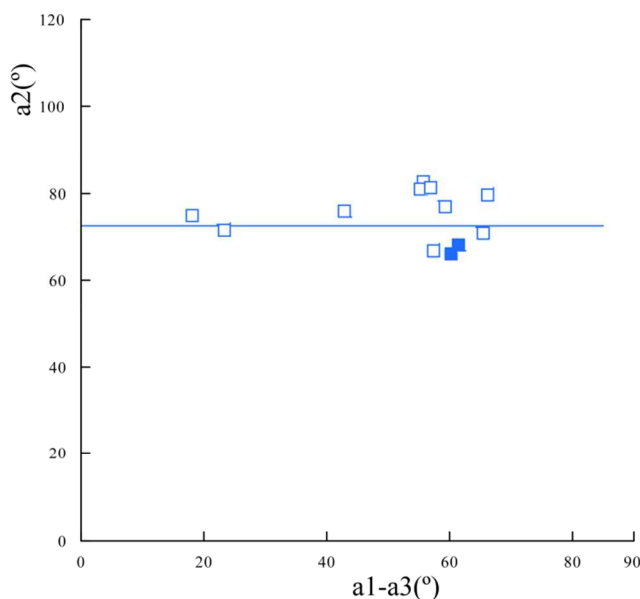


Fig. 3 Representation of a_2 parameter vs a_1-a_3 parameter for compounds in Table 3. Compound **1** and **2** are marked in dark.

In order to have an holistic view of the question (including the effect of distances) dA/dB and dA/dB^* values have been represented vs $a_2/(a_1-a_3)$ parameter (Fig. 4). As observed, the change of dA/dB and dA/dB^* with $a_2/(a_1-a_3)$ parameter is similar. Thus, values of dA/dB decrease for decreasing values of $a_2/(a_1-a_3)$, the slope becoming abrupt when $a_2/(a_1-a_3)$ tends to 1 (this is, the value for the ideal 3-c herringbone).

The general trend observed in figure 4 should be corroborated with more structural data. Thus, our contribution is the identification of the structural parameters defining a 3-c herringbone array, and the proposal of a correlation between angles and distances in this type of structures.

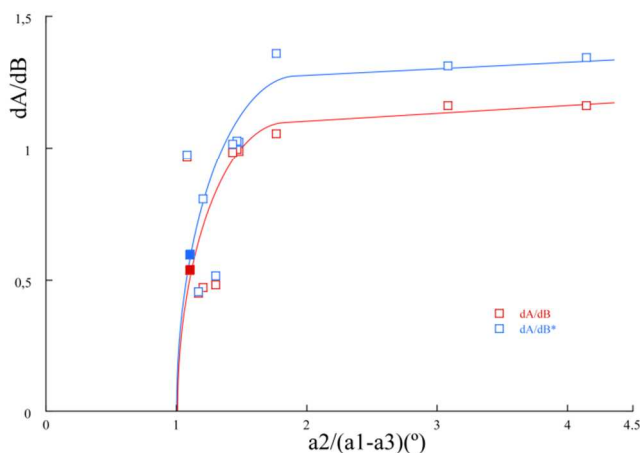


Fig. 4 Representation of dA/dB and dA/dB^* values vs $a_2/(a_1-a_3)$ parameter for compounds in table 3. Compounds **1** and **2** are marked in dark.

Electronic Paramagnetic Resonance

X and Q band EPR measurements were carried out on powdered samples at several temperatures in the range 5-300 K. Due to the structural similarities in compounds **1** and **2**, compound **1** was selected for measurements, as it exhibits two crystallographically independent metal atoms. The X-band powder EPR spectrum of compound **1** shows the characteristic shape of Cu^{II} sites with axial symmetry, remaining practically unchanged from RT down to 5 K. However, operating at Q-band, a rhombic signal is observed (Fig. 5).

The spin Hamiltonian parameters were estimated by comparison of the experimental spectra with those obtained by a computer simulation program working at the second order of the perturbation theory. The parameters were optimized by the trial and error method and the best-fit results are represented as dashed lines in figure 5. The principal components of the g-tensor are $g_1 = 2.261$, $g_2 = 2.103$ and $g_3 = 2.062$ ($g_{\text{iso}} = 2.142$). The absence of hyperfine structure is indicative of the magnetic exchange between non equivalent Cu^{II} ions.

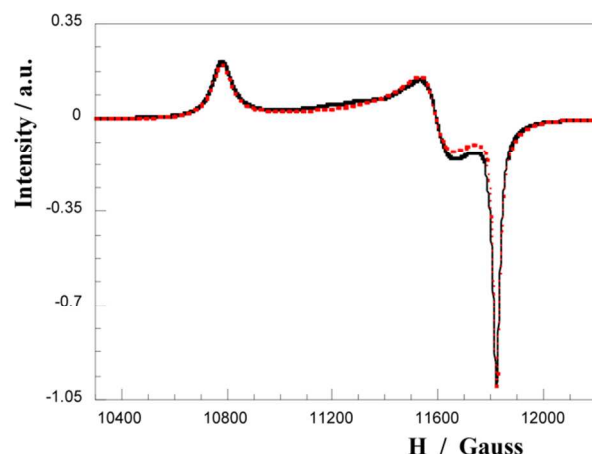


Fig. 5 Q and EPR spectrum for compound **1**.

Magnetic properties

The thermal variation of the inverse of the magnetic molar susceptibility (χ_m^{-1}) and the $\chi_m T$ product ($\mu_{\text{eff}}^2 = 8\chi_m T$) for compound **1** is shown in figure 6.

The effective magnetic moment exhibits a plateau from RT to 20 K having a value of 2.6 μ_B , decreasing to a value of 2.3 μ_B at 5 K. Above 10 K, the magnetic susceptibility follows a Curie-Weiss law with $C_m = 0.85 \text{ cm}^3 \cdot \text{Kmol}^{-1}$ and $\theta = -1.4 \text{ K}$. Both, the negative temperature intercept and the decrease of the magnetic effective moment at low temperatures are in agreement with weak antiferromagnetic interactions in the compound (in accordance with EPR analysis).

20

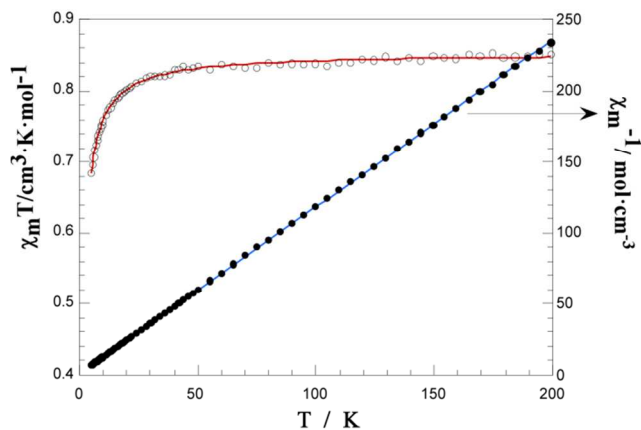


Fig. 6 Temperature dependence of $\chi_m T$ of compound 1.

According to the structural features, the magnetic measurements on **1** have been fitted by the Bonner and Fisher's expression (Eq.1) for chains of equally spaced copper(II) ions derived from the Heisenberg-van Vleck-Dirac Hamiltonian for isotropic magnetic 1D systems with $S = \frac{1}{2}$ spins (Eq. 2).^{52,53} The best least-square fitting was achieved for $J/k = -0.95$ K (0.66 cm⁻¹) and calculated $g = 2.13$ (experimental EPR value is 2.14).

$$X_m = \frac{Ng^2\beta^2}{KT} \frac{0.25 + 0.074975x + 0.075235x^2}{1 + 0.9931x + 0.172135x^2 + 0.757825x^3} \quad (\text{Eq. 1})$$

$$H = -2J \sum_{i=1}^{n-1} S_{Ai} \cdot S_{AiH} \quad (\text{Eq. 2})$$

Where

$$x = \frac{|2J|}{KT}$$

Conclusions

Combination of PDC and bpe ligands to produce SCFs (also known as MOFs) has been poorly explored, so far. In this scope, we have prepared two 2D compounds using these ligands, and Cu^{II} as a metal node. Both compounds exhibit similar structural features consisting of herringbone arrays, and solvent molecules located in between. These crystallization molecules provide the hydrogen bonds that stabilize the 3D framework. The fact that similar 3D arrays are produced with different solvent molecules is indicative of the flexibility of this type of compounds.

The use of the term "herringbone" in literature is wide and can lead to confusion, so we have identified two types of herringbone-arrays (4-c and 3-c) depending on the number of connections for each metal node. This way, M₁A₁B₁ stoichiometry corresponds to 4-c arrays, while M₂A₂B stoichiometry corresponds to 3-c ones (M is the metal ion, and A and B are the organic ligands).

We have also identified the structural parameters defining the 3-c herringbone arrays (the one adopted by the compounds reported in this work), and have observed a correlation between angles and distances in this type of structures. Finally, we have studied a set of compounds self-named as herringbone networks, and have found that the M-A-M zig-zag chain exhibit values close to 74° for all the cases.

Acknowledgements

This work has been financially supported by the "Ministerio de Economía y Competitividad" (MAT2013-42092-R) and the "Gobierno Vasco" (Basque University System Research Group, IT-630-13) which we gratefully acknowledge. SGIker (UPV/EHU) technical support (MEC, GV/EJ, and European Social Fund) is gratefully acknowledged. F. Llano-Tomé thanks the "Ministerio de Ciencia e Innovación" for a fellowship (BES-2011-045781).

Notes and references

- H. Furukawa, K. E. Cordova, M. O'Keeffe and O. M. Yaghi, *Science*, 2013, **341**, 974.
- M. O'Keeffe and O. M. Yaghi, *Chem. Rev.*, 2012, **112**, 675-702.
- M. Li, D. Li, M. O'Keeffe and O. M. Yaghi, *Chem. Rev.*, 2014, **114**, 1343-1370.
- T. R. Cook, Y.-R. Zheng and P. J. Stang, *Chem. Rev.*, 2013, **113**, 734-777.
- C. Wang, D. Liu and W. Lin, *J. Am. Chem. Soc.*, 2013, **135**, 13222-13234.
- F. Gandara, H. Furukawa, S. Lee and O. M. Yaghi, *J. Am. Chem. Soc.*, 2014, **136**, 5271-5274.
- D. J. Tranchemontagne, K. S. Park, H. Furukawa, J. Eckert, C. B. Knobler and O. M. Yaghi, *J. Phys. Chem. C*, 2012, **116**, 13143-13151.
- T. A. Makal, J.-R. Li, W. Lu and H.-C. Zhou, *Chem. Soc. Rev.*, 2012, **41**, 7761-7779.
- Z. Zhang, Y. Zhao, Q. Gong, Z. Li and J. Li, *Chem. Commun.*, 2013, **49**, 653-661.
- P. Nugent, Y. Belmabkhout, S. D. Burd, A. J. Cairns, R. Luebke, K. Forrest, T. Pham, S. Ma, B. Space, L. Wojtas, M. Eddaoudi and M. J. Zaworotko, *Nature*, 2013, **495**, 80-84.
- B. Liu, S. Jie and B. Li, *Huaxue Jinzhan*, 2013, **25**, 36-45.
- J. Gascon, A. Corma, F. Kapteijn and F. X. Llabres i Xamena, *ACS Catal.*, 2014, **4**, 361-378.
- J. E. Mondloch, O. K. Farha and J. T. Hupp, *RSC Catal. Ser.*, 2013, **12**, 289-309.
- H. R. Moon, D.-W. Lim and M. P. Suh, *Chem. Soc. Rev.*, 2013, **42**, 1807-1824.
- J. Zhuang, C.-H. Kuo, L.-Y. Chou, D.-Y. Liu, E. Weerapana and C.-K. Tsung, *ACS Nano*, 2014, **8**, 2812-2819.
- M. C. Bernini, D. Fairen-Jimenez, M. Pasinetti, A. J. Ramirez-Pastor and R. Q. Snurr, *J. Mater. Chem. B*, 2014, **2**, 766-774.
- P. Horcajada, T. Chalati, C. Serre, B. Gillet, C. Sebrie, T. Baati, J. F. Eubank, D. Heurtaux, P. Clayette, C. Kreuz, J.-S. Chang, Y. K. Hwang, V. Marsaud, P.-N. Bories, L. Cynober, S. Gil, G. Férey, P. Couvreur and R. Gref, *Nat. Mater.*, 2010, **9**, 172-178.
- Z. Hu, J. D. Benjamin and J. Li, *Chem. Soc. Rev.*, 2014.
- L. E. Kreno, K. Leong, O. K. Farha, M. Allendorf, R. P. Van Duyne and J. T. Hupp, *Chem. Rev.*, 2012, **112**, 1105-1125.
- G. Lu and J. T. Hupp, *J. Am. Chem. Soc.*, 2010, **132**, 7832-7833.
- J. C. Rybak, M. Hailmann, P. R. Matthes, A. Zurawski, J. Nitsch, A. Steffen, J. G. Heck, C. Feldmann, S. Goetzendoerfer, J. Meinhardt, G. Sxthl, H. Kohlmann, S. J. Sedlmaier, W. Schnick and K. Mueller-Buschbaum, *J. Am. Chem. Soc.*, 2013, **135**, 6896-6902.
- C.-Y. Sun, X.-L. Wang, X. Zhang, C. Qin, P. Li, Z.-M. Su, D.-X. Zhu, G.-G. Shan, K.-Z. Shao, H. Wu and J. Li, *Nat. Commun.*, 2013, **4**, 2717.
- P. Horcajada, R. Gref, T. Baati, P. K. Allan, G. Maurin, P. Couvreur, G. Férey, R. E. Morris and C. Serre, *Chem. Rev.*, 2012, **112**, 1232-1268.
- J. Wack, R. Siegel, T. Ahnfeldt, N. Stock, L. Mafrá and J. Senker, *J. Phys. Chem. C*, 2013, **117**, 19991-20001.
- A. Calderon-Casado, G. Barandika, B. Bazan, M.-K. Urriaga and M.-I. Arriortua, *CrystEngComm*, 2013, **15**, 5134-5143.

26. A. Calderon-Casado, G. Barandika, B. Bazan, M.-K. Urtiaga, O. Vallcorba, J. Rius, C. Miravittles and M.-I. Arriortua, *CrystEngComm*, 2011, **13**, 6831-6838.
27. A. Calderon-Casado, G. Barandika, B. Bazan, M.-K. Urtiaga and M.-I. Arriortua, *CrystEngComm*, 2010, **12**, 1784-1789.
28. A. Calderon-Casado, G. Barandika, B. Bazan, M.-K. Urtiaga and M.-I. Arriortua., *PCT Int. Appl.* 2013, WO 2013057350 A1 20130425.
29. Z.-G. Li, G.-H. Wang, H.-Q. Jia, N.-H. Hu, J.-W. Xu and S. R. Batten, *CrystEngComm*, 2008, **10**, 983-985.
30. L.-L. Wen, D.-B. Dang, C.-Y. Duan, Y.-Z. Li, Z.-F. Tian and Q.-J. Meng, *Inorg. Chem.*, 2005, **44**, 7161-7170.
31. A. J. Blake, N. R. Brooks, N. R. Champness, M. Crew, L. R. Hanton, P. Hubberstey, S. Parsons and M. Schroder, *J. Chem. Soc., Dalton Trans.*, 1999, 2813-2817.
32. Z. He, Z.-M. Wang and C.-H. Yan, *CrystEngComm*, 2005, **7**, 143-150.
33. W. Zheng, X. Liu, J. Guo, L. Wu and D. Liao, *Inorg. Chim. Acta*, 2004, **357**, 1571-1578.
34. J. Lin, L. Wen, S. Zang, Y. Su, Z. Lu, H. Zhu and Q. Meng, *Inorg. Chem. Commun.*, 2007, **10**, 74-76.
35. C. M. Rogers, N. H. Murray, R. M. Supkowski and R. L. La Duca, *Inorg. Chim. Acta*, 2013, **407**, 167-174.
36. E. Shyu, M. A. Braverman, R. M. Supkowski and R. L. LaDuca, *Inorg. Chim. Acta*, 2009, **362**, 2283-2292.
37. S. Sengupta, S. Ganguly, A. Goswami, P. K. Sukul and R. Mondal, *CrystEngComm*, 2013, **15**, 8353-8365.
38. D.-C. Wen, S.-X. Liu and J. Ribas, *Inorg. Chem. Commun.*, 2007, **10**, 661-665.
39. M. A. Withersby, A. J. Blake, N. R. Champness, P. A. Cooke, P. Hubberstey and M. Schroder, *New J. Chem.*, 1999, **23**, 573-575.
40. W.-L. Meng, Z.-H. Zhang, Y. Lv, H. Kawaguchi and W.-Y. Sun, *Appl. Organomet. Chem.*, 2006, **20**, 399-403.
41. M. Kondo, M. Shimamura, S. I. Noro, S. Minakoshi, A. Asami, K. Seki and S. Kitagawa, *Chem. Mater.*, 2000, **12**, 1288-1299.
42. M. A. Withersby, A. J. Blake, N. R. Champness, P. A. Cooke, P. Hubberstey, A. L. Realf, S. J. Teat and M. Schroder, *Dalton*, 2000, 3261-3268.
43. W. Yinghua, *J. Appl. Crystallogr.*, 1987, **20**, 258-259.
44. A. Altomare, G. Cascarano, C. Giacovazzo and A. Guagliardi, *J. Appl. Crystallogr.*, 1993, **26**, 343-350.
45. G. M. Sheldrick, *Acta Crystallogr., Sect. A Found. Crystallogr.*, 2008, **64**, 112-122.
46. V. A. Blatov, *IUCr CommpComm Newsl.* **7**, 2006, 4-38. <http://www.topos.ssu.samara.ru>.
47. H. Zabrodsky, S. Peleg and D. Avnir, *J. Am. Chem. Soc.*, 1992, **114**, 7843-7851.
48. M. Pinsky and D. Avnir, *Inorg. Chem.*, 1998, **37**, 5575-5582.
49. D. C. M. Llunell, J. Cirera, J. M. Bofill, P. Alemany, S. Álvarez, M. Pinsky and D. Yanutir, *SHAPE v1.1a*, 2003.
50. S. Álvarez, P. Alemany, D. Casanova, J. Cirera, M. Llunell and D. Avnir, *Coord. Chem. Rev.*, 2005, **249**, 1693-1708.
51. "Powder Diffraction File - Inorganic and Organic", ICCD, Pennsylvania.Ref.Code: 01-080-1268, 2001.
52. O. Khan, *Molecular Magnetism*, VCH Publishers, Weinheim, 1993.
53. J. C. Booner and M. E. Fisher *Phys. Rev. B*, 1964, **135**.